Infrared observation of the phase transitions of ice at low temperatures and pressures up to 50 GPa and the metastability of low-temperature ice VII

M. Song
Core Research for Evolutional Science and Technology, Japan Science and Technology Corporation, Kawaguchi, Saitama 332-0012, Japan

H. Yamawaki, H. Fujihisa, M. Sakashita, and K. Aoki
National Institute of Advanced Industrial Science and Technology, Tsukuba Central 5, Tsukuba 305-8565, Japan
(Received 3 March 2003; published 31 July 2003)

The phase transitions of H_2O ice were investigated by infrared-absorption measurements in the *P, T* ranges of 0.2–50 GPa and 20–298 K. Under compression at temperatures below 150 K, ices II and VI were found to transform directly into orientationally disordered low-temperature ice VII due to their mechanical instability, with the transition pressure increasing approximately from 2.8 GPa at 120 K to 7.9 GPa at 40 K. The infrared spectral features of low-temperature ice VII are identical to those of ice VII at ambient temperature. Under isobaric heating in the range of 100 to 180 K at pressures below 30 GPa, low-temperature ice VII transforms into fully ordered antiferroelectric ice VIII; during this transition, the water molecules reorient by rotation. The kinetic phase boundary between low-temperature ice VII and ice VIII at temperatures below 100 K was determined to be a vertical line at about 30 GPa. The low-temperature ice VII to ice VIII transition is interpreted here as occurring as a result of thermally activated rotational disordering below 30 GPa and as a result of rotational tunneling coupled with bending vibrations above 30 GPa; the orientational disordering of ice VII can be explained accordingly.

DOI: 10.1103/PhysRevB.68.024108 PACS number(s): 64.70.Kb, 62.50.+p, 78.30.−j

I. INTRODUCTION

The high-pressure behavior of ice is of fundamental importance to condensed-matter physics and the planetary sciences. Many intriguing phenomena have been discovered in the high-pressure behavior of ice, such as pressure-induced amorphization,[1,2] hydrogen-bond symmetrization or centering,[3–5] as well as Fermi resonance and soft-mode behavior.[4,6–8] At ambient temperature and pressures above 2 GPa, ice crystallizes as body-centered-cubic (bcc) ice VII ($Pn3m$), in which the H_2O molecules are orientationally disordered.[9] A recent diffusion experiment indicated that molecules in ice VII can rotate dynamically at 400 K.[10] With decreasing temperature, ice VII transforms into tetragonal ice VIII ($I4_1/amd$), in which the molecules are oriented in a fully ordered antiferroelectric configuration.[9] The crystal structures of ices VII and VIII are very similar, and ice VII can be understood as a disordered analog of ice VIII, despite the slight tetragonal distortion in the *c* axis of ice VIII.[9,11,12] Under high compression, the molecular phases VII and VIII transform into translationally disordered ice X (ionized phase) at about 60 GPa due to translational proton tunneling and then at about 100 GPa transform into fully centered ice X (atomic phase), which is predicted to have a Cu_2O cuprite structure in which the protons are definitely located at the hydrogen-bond midpoints.[3–5,7,8,13–15]

The physical properties of ice are especially unusual in the low-temperature and low-pressure region. When pressurized at 77 K, ice Ih transforms into high-density amorphous (HDA) ice at 1.0 GPa due to its mechanical instability.[1,2,16] Raman-scattering measurements have been used to show that HDA ice transforms into an ice-VII-like phase at about 4 GPa at 77 K.[2] Recent neutron-diffraction measurements confirmed that ice-VII-like phases (here called low-temperature (LT) ice VII and denoted as LT VII in the figures) can also be made by compressing ices II and VI up to 4 GPa at low temperatures and they possess the same crystal structure as ice VII.[17–21] Low-temperature ice VII is similar to ice VIII in that it can be quenched as a metastable phase to ambient pressure below 100 K, and then it undergoes successive transitions to low-density amorphous ice and ice Ih upon heating.[19] Since thermal effects on molecular rotation are not expected at temperatures below 100 K, orientational disordering is static in low-temperature ice VII, which is different from the dynamic orientational disordering found in ice VII. When heated at pressures above 2 GPa, low-temperature ice VII transforms into ice VIII. Theoretical calculations have predicted that low-temperature ice VII should transform into ice VIII under isothermal compression,[22] but Raman measurements found no phase transformation at pressures up to 30 GPa at 77 K (Ref. 2).

Vibrational spectroscopy provides promising tools for detecting the vibrational dynamics and structural transformations of molecular solids. Here we present an infrared (IR) -absorption study of the low-temperature phase transitions of H_2O ice and of the metastability of low-temperature ice VII. Unlike the phase transitions from the molecular phases VII and VIII into translationally disordered ice X and further into fully centered ice X, which are dominated by translational proton motion along the hydrogen-bonded O-O axis, the phase transition from low-temperature ice VII into ice VIII involves reorientation of the H_2O molecules by rotation from a static orientationally disordered paraelectric to a fully ordered antiferroelectric configuration. A study of the metastability of low-temperature ice VII should deepen our understanding of the mechanism of this phase transition, and shed

light on the nature of orientational disordering in ice VII. Further investigation of the phase transitions of ice at low temperatures and pressures should also be helpful for understanding the unusual phase-transition behavior in this *P-T* region.

II. EXPERIMENTAL PROCEDURE

Low-temperature and high-pressure IR measurements were carried out with a Fourier-transform-IR spectrometer, a CuBe membrane diamond-anvil cell (MDAC), and a closed-cycle cryogenic refrigerator system with KBr windows. A thin film of H_2O ice roughly 1-μm thick was prepared inside the MDAC by the vapor-deposition method in order to avoid saturation of the strong IR-absorption peaks of ice. The ice film, the KBr pressure medium, and ruby grains were placed in the sample chamber inside the cell in a sandwich configuration. The sampling process was conducted in a glove box purged with nitrogen gas, with the cell cooled to approximately 260 K by liquid nitrogen.

After sampling, the cell was put into the cryostat and cooled under vacuum conditions of about 10^{-6}–10^{-7} Torr. A resistive heater and a diode thermal sensor were placed near the cell for controlling and monitoring the temperature inside the cryostat. The sample temperature was measured with an Au+0.07%Fe-Cr thermocouple fixed on the surface of one diamond anvil with Stycast cement. The sample pressure was controlled by regulating the helium gas pressure in the membrane and determined by the quasihydrostatic ruby scale.[23] Zero-pressure reference spectra of ruby at low temperatures were measured *in situ* with ruby grains fixed to the back surface of one diamond anvil. IR spectra were acquired over a wave-number range of 650–6700 cm^{-1} with a resolution of 4 cm^{-1}. The measured sample area was trimmed to a square of about 30×30 μm^2 with an adjustable optical mask. IR spectra were measured for both an empty MDAC at ambient pressure and a KBr-filled MDAC at high pressures and used as a correction for diamond absorption.[8]

The infrared spectra of ice were obtained for the *P*, *T* ranges of 0.2–50 GPa and 20–298 K. First, we carefully examined the IR spectra of the crystalline ices Ih, II, V, VI, VII, and VIII and compared them with the previous IR data of these phases.[24–28] Each phase could be readily identified by its characteristic rotational, bending, and stretching bands. Then we unloaded the MDAC to 0.2–1 GPa in the temperature range 230–240 K in order to make ice II or VI, both of which can be cooled to temperatures below 120 K without phase changes. Low-temperature ice VII was made by isothermally compressing ice II or VI to 4–10 GPa at temperatures below 100 K and its metastability was investigated along both isothermal and isobaric paths.

III. RESULTS

The phase transitions from ices II and VI into low-temperature ice VII were investigated at temperatures below 120 K along isothermal paths. Figure 1 shows two sets of spectra, one measured along the 120-K isotherm (top panel) and the other along the 40-K isotherm (lower panel). In the top panel, the 0.2-, 1.3-, and 2.2-GPa spectra are assigned to ice II by reference to the IR spectra of the crystalline phases of ice published previously and to those observed in this work.[24–28] The stretching and bending vibrational peaks are located at approximately 3300 and 1700 cm^{-1}, respectively, and two rotational peaks are located at approximately 670 and 800 cm^{-1} (marked by short bars). As the pressure increases from 2.2 to 3.5 GPa, the stretching frequency shows a discontinuous increase, and the two rotational peaks disappear and evolve into an absorption shoulder. These spectral changes are attributed here to the transition from ice II to low-temperature ice VII on the basis of previous neutron-diffraction measurements and the results of the present study.[17–20] The vibrational modes of low-temperature ice VII were assigned by following the mode assignment for ice VII.[7,8,27] In the lower panel of Fig. 1 (the 40-K isotherm), the 0.2-GPa spectrum is assigned to ice VI. The phase transition from ice VI to low-temperature ice VII was observed to occur as the pressure increased from 7.6 to 8.2 GPa, with similar spectral changes to those of the ice-II to the low-temperature ice-VII transition. The pressures of the phase transitions from ices II and VI to low-temperature ice VII are plotted in Fig. 2. The phase-transition pressures show a general trend of increasing with decreasing temperature, from ~2.8 GPa at 120 K to ~7.9 GPa at 40 K.

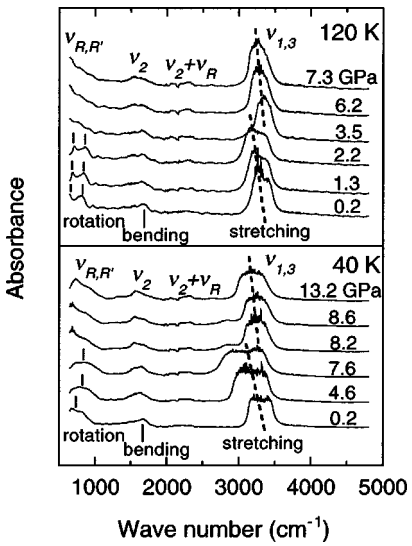

FIG. 1. Infrared spectra for the ice-II to low-temperature ice-VII transition at 120 K (top panel) and the ice-VI to low-temperature ice-VII transition at 40 K (lower panel). Both phase transitions feature a discontinuous increase in the stretching frequency and a disappearance of the rotational peaks (marked by short bars). $\nu_{1,3}$ denotes the symmetric and asymmetric stretching vibrational modes, ν_2 the bending vibrational mode, $\nu_{R,R'}$ the rotational vibrational modes, and $\nu_2+\nu_R$ the combination of the ν_2 and ν_R vibrational modes. Dashed lines are guides only.

Low-temperature ice VII and its metastable field were investigated by isothermal compression below 100 K. Figure 3 presents a set of representative spectra obtained along a 75-K isothermal path for pressures up to 37 GPa. The 0.32-GPa spectrum was assigned to ice II (see also Fig. 1). The ice-II to low-temperature ice-VII transition occurs as the pressure

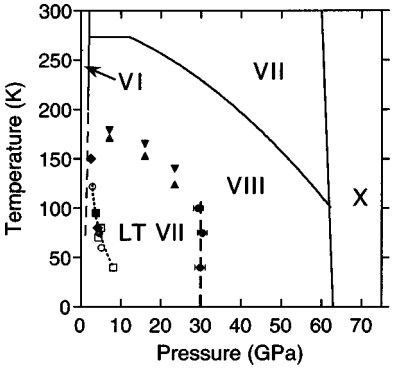

FIG. 2. Low-temperature phase transitions observed in the present IR measurements. Open squares indicate the ice-VI to low-temperature ice-VII transition; open circles denote the ice-II to low-temperature ice-VII transition; solid triangles denote the low-temperature ice-VII to ice-VIII transition along isobaric warming paths (up and down triangles represent the onset and completion points of the transition, respectively); solid circles are the low-temperature ice-VII to ice-VIII transition along isothermal paths. The diamonds and the solid square are the previously reported HDA and ice-VI to low-temperature ice-VII transition points, respectively (Refs. 2 and 19). The phase boundaries for ices VII, VIII, and X (nonmolecular phase) were drawn according to previous Raman-scattering and IR measurements (Refs. 5, 8, 13, and 28). Low-temperature ice VII is denoted as LT VII in the figure. Dashed lines are guides only.

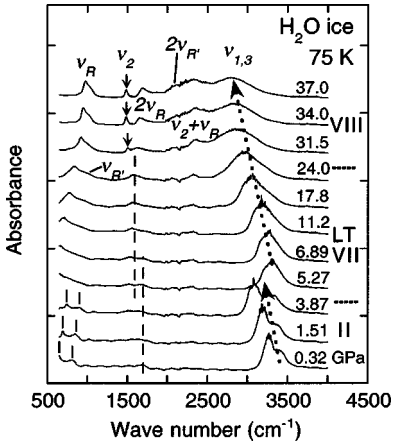

FIG. 3. Infrared spectra of H_2O ice for pressures up to 37 GPa measured along the 75-K isotherm. The spectra below 4 GPa are assigned to ice II. As the pressure increases from 3.87 to 5.27 GPa, ice II transforms into low-temperature ice VII with a discontinuous shift of the stretching $\nu_{1,3}$ peak and the disappearance of the two rotational peaks (marked by short bars). Significant spectral changes at around 30 GPa indicate a phase transition from low-temperature ice VII into ice VIII. A new sharp peak appears at approximately 1500 cm^{-1} (marked by short arrows) in the spectra for pressures above 30 GPa, being assigned as the ν_2 bending vibrational peak of ice VIII. This ν_2 bending vibrational peak at ~ 1500 cm^{-1} is related to the out-of-phase ν_{2-} bending vibration of the ν_2 bending mode of ice VIII (see details in Sec. IV and Fig. 6). Denotations of the vibrational modes are the same as in Fig. 1, and $2\nu_R$ and $2\nu_{R'}$ are the overtones of the rotational vibrational modes. Low-temperature ice VII is denoted as LT VII. Dashed arrows and lines are guides only.

increases from 3.87 to 5.27 GPa. The spectral features of low-temperature ice VII are quite similar to those observed for ice VII at room temperature. The peak frequencies of the vibrational modes of ice observed at 75 K are plotted as a function of pressure in Fig. 4. The frequency-pressure curves of the vibrational modes of low-temperature ice VII are nearly identical to those of the corresponding modes of ice VII for pressures up to 30 GPa. As the pressure increases from 5 to 30 GPa, the $\nu_{1,3}$ stretching frequency of low-temperature ice VII softens and the $\nu_{R,R'}$ rotational frequencies harden, but the ν_2 bending frequency remains constant at 1570 cm^{-1}.

Significant spectral changes were observed at around 30 GPa. The ν_2 bending mode of low-temperature ice VII, located near 1570 cm^{-1} at pressures below 30 GPa, shifts to approximately 1500 cm^{-1} as the pressure increases above 30 GPa. In addition, at pressures above 30 GPa the absorption peaks of the vibrational modes become obviously sharper than those in the spectra obtained below 30 GPa. A frequency shift of the ν_2 bending mode around 30 GPa was also observed in the experimental runs along the 40- and 100-K isotherms, as depicted in Fig. 5. The frequency of the IR-active bending vibrational mode has previously been found to be sensitive to the ice-VII to ice-VIII transition.[28] For this reason, IR data from the bending vibrational region for ices VII and VIII was also plotted in Fig. 5. For all three experimental runs along the 40-, 75-, and 100-K isotherms, the ν_2 bending frequencies trace the frequency-pressure curve (at about 1570 cm^{-1}) of the bending mode for ice VII up to 30 GPa, but deviate from those of ice VII and suddenly shift toward those of the bending frequency-pressure curve (at 1480 cm^{-1}) for ice VIII at pressures above 30 GPa.[29] For the 40- and 75-K isotherms, the bending frequencies are a little higher than those of ice VIII at pressures just above 30 GPa but become almost the same as those of ice VIII near 40 GPa. The spectral changes at 30 GPa are hence interpreted as due to the low-temperature ice-VII to ice-VIII transition.

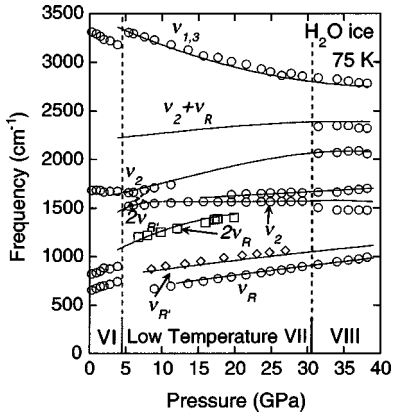

FIG. 4. The pressure dependence of the frequencies of the IR-active vibrational modes for H_2O ice measured along the 75-K isotherm (open circles). Open squares and diamonds are data for low-temperature ice VII measured at 40 and 100 K, respectively. Previous data for ice VII at room temperature are drawn as solid lines (Refs. 8 and 28).

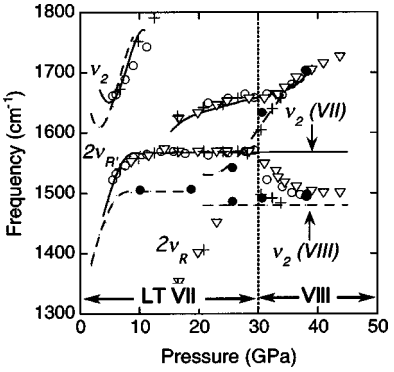

FIG. 5. Variations of the vibrational peak frequencies of H_2O ice for pressures up to 45 GPa in the bending vibrational region. Crosses are the data measured at 100 K; open circles, 75 K; open triangles, 40 K; solid circles, 75 K (unloading). Solid and dashed lines are previous data for ice VII and VIII, respectively (Refs. 8 and 28). Low-temperature ice VII is denoted as LT VII.

This was additionally confirmed during the unloading process from 40 to 10 GPa at 75 K, during which the observed peak frequencies are identical to those of ice VIII. Below 100 K, the kinetic phase boundary between low-temperature ice VII and VIII was found to be a vertical line at 30 GPa, i.e., insensitive to temperature (Fig. 2).

The metastable field of low-temperature ice VII was also explored as a function of temperature along isobaric warming paths at 6, 15, and 23 GPa (Fig. 2). The rate of temperature increase was set at approximately 0.1 K/min. The phase transition into ice VIII was determined mainly by the spectral changes in the bending vibrational region. During the 6-GPa isobaric run, low-temperature ice VII transforms into ice VIII over the temperature span of 170–180 K. At higher pressures, this phase transition becomes sluggish and takes place over a wider temperature span. For the 23-GPa isobaric run, low-temperature ice VII begins to transform into ice VIII at about 120 K and is completely converted into ice VIII by 140 K. The transition temperatures determined in these isobaric runs exhibit a general trend of decreasing with pressure.

IV. DISCUSSION

Under compression at 77 K, ice Ih transforms into HDA at about 1.0 GPa and then into low-temperature ice VII at about 4 GPa.[1,2] Unlike ice Ih, ices II and VI transform into low-temperature ice VII directly when compressed at temperatures below 150 K. Low-temperature ice VII possesses essentially the same crystal structure as ice VII ($Pn3m$), composed as it is of two hydrogen-bonded Ic networks with disordered protons and of oxygen atoms forming a bcc sublattice.[9] Ice VI ($P4_2/nmc$) is also composed of two Ic networks with disordered protons, but its oxygen atoms form a tetragonal sublattice.[9] Ice II consists of only one Ic network, with ordered protons and its oxygen atoms form a rhombohedral sublattice ($C222_1$).[30] Thus the phase transitions from ices II and VI to low-temperature ice VII involve structural changes, which are accompanied by density increases of about 25%–45%. As mentioned above, these phase transitions feature a discontinuous increase of the $\nu_{1,3}$ stretching frequency (Figs. 1 and 2). In contrast to the density increase, this frequency increase implies that an increase of the hydrogen-bonded O-O distance has occurred, which is suggested by the correlation between the decoupled O-H vibrations and the hydrogen-bond length.[31,32]

At temperatures between 200 and 273 K, ice VI transforms into ice VIII at 1.9–2.1 GPa. Compressing ice VI below 150 K leads to no phase change at pressures around the extrapolated ice VI/ice VIII boundary (about 0.8–1.5 GPa). However, transitions into low-temperature ice VII were observed at higher pressures. The pressure at which the ice-VI to low-temperature ice-VII transition occurs is observed to increase with decreasing temperature, from ~2.8 GPa at 120 K to ~7.9 GPa at 40 K. These features are very similar to the amorphization of ice Ih into HDA ice, in which the amorphization mechanism changes from thermodynamic melting for $T>162$ K to mechanical melting at lower temperatures.[16] By analogy, the ice VI to VIII transition at 200–270 K is perhaps best understood as a thermodynamic transition, whereas below about 150 K the ice-VI to low-temperature ice-VII transition is best understood as occurring as a result of mechanical instability due to the violation of the Born stability condition $C_{11}-|C_{12}|>0$.[16] The two transitions ice II to low-temperature ice VII and HDA to low-temperature ice VII, which occur at almost the same pressure and temperature as the ice-VI to low-temperature ice-VII transition, thus also have a mechanical instability mechanism.

Low-temperature ice VII possesses essentially the same crystal structure as ice VII ($Pn3m$).[19] In the present study it was observed that the IR spectroscopic features of low-temperature ice VII are identical to those of ice VII at room temperature for pressures up to 30 GPa, indicating that there are no structural differences between the two phases. Multisite disordering of O and H atoms, which is found in ice VII at ambient temperature, may also be present in low-temperature ice VII.[12] In ice VII, the orientations of molecules are dynamically disordered, and all four covalent proton positions around each oxygen atom are occupied with 50% probability by two protons. As the dynamics of proton motion slows substantially with decreasing temperature and the protons become effectively frozen below 100 K,[33,34] the orientational disordering in low-temperature ice VII is believed to become static.[19] Ices VII and VIII possess very close crystal structures composed of two hydrogen-bonded Ic networks. As mentioned above, ice VII can be taken as a disordered analog of ice VIII, despite the slight tetragonal distortion in the c axis of ice VIII.[9,11] Thus the phase transition from low-temperature ice VII into ice VIII with a fully ordered antiferroelectric configuration involves molecular reorientation by rotation and a displacement between the two hydrogen-bonded Ic networks. The energy barrier for the rotational motion of molecules in ice is low according to theory.[35] At pressures below 30 GPa, low-temperature ice VII transforms into ice VIII under isobaric heating. This implies that molecular reorientation by rotation below 30 GPa is in fact a thermally activated process. The most reasonable explanation of the low-temperature ice-VII to ice-VIII transition is that the orientational disorder in low-temperature ice

VII becomes dynamical and the two Ic networks are displaced due to short-range dipole-dipole interaction of water molecules. Hence we infer here that with increasing temperature the ''frozen'' disorder in low-temperature ice VII becomes thermally activated rotational disordering, which is the premise for the transition into ice VIII, and then this rotational disordering disappears as low-temperature ice VII transits into fully ordered antiferroelectric ice VIII at pressures below 30 GPa. Under compression, the O-H covalent bond length does not increase significantly up to 30 GPa, while the hydrogen-bonded O-O distance decreases from 2.98 Å at 0 GPa to 2.54 Å at 30 GPa.[11,36] This indicates that the dipole-dipole interaction in low-temperature ice VII is enhanced with increasing pressure. The enhancement of the dipole-dipole interaction with pressure in low-temperature ice VII contributes to the kinetic process of molecular reorientation into the ordered ice VIII and allows the transition into ice VIII to take place at lower temperature at higher pressure. This explains the negative slope of the kinetic phase boundary for the low-temperature ice-VII to ice-VIII transition, as was observed for pressures below 30 GPa.

At temperatures below 100 K the kinetic phase boundary between low-temperature ice VII and ice VIII is determined as a vertical line at 30 GPa, i.e., it is temperature insensitive. This vertical phase line is very similar to the ice VIII/ice X boundary near 60 GPa; transition between these two phases is caused by translational tunneling of protons, and depends mainly on the hydrogen-bonded O-O distance.[3–5,13] As mentioned above, the low-temperature ice-VII to ice-VIII transition mainly involves the rotation of molecules, so therefore the vertical phase line for the low-temperature ice-VII to ice-VIII transition is interpreted here to be a result of rotational tunneling, which is also dominated by the hydrogen-bonded O-O distance. Here thermal effects on the O-O distance can be neglected. For the 40- and 70-K isothermal runs, the bending frequencies above 30 GPa slightly deviate from but gradually become close to those of ice VIII at 1480 cm^{-1} with compression up to 40 GPa. This deviation is explained as resulting from the difference of the displacements between the two hydrogen-bonded Ic networks from those of the normal ice VIII. Here we relate bending frequency to the displacement between two Ic networks.[28]

Careful examination of the spectra of ice VIII reveals that the bending mode splits at pressures above 23 GPa (Fig. 6, top panel). The bending mode that appears as a single peak at 1500 cm^{-1} at pressures below 23 GPa splits into two peaks in the 23.7-GPa spectrum, one at 1480 cm^{-1} and another at 1530 cm^{-1}, which are assigned as out-of-phase ν_{2-} and in-phase bending ν_{2+} vibrations, respectively.[37] Under further compression, the out-of-phase bending peak remains at 1480 cm^{-1}, but its peak width becomes obviously sharper than the single bending peak that is found at pressures below 23 GPa. For ice VII, bending mode splitting was also observed and can be clearly recognized at pressures above 26 GPa (Fig. 6, lower panel). In the 26.1-GPa spectrum, the peaks of the out-of-phase ν_{2-} and in-phase ν_{2+} bending vibrations are located at 1570 and 1640 cm^{-1}, respectively. Under further compression, the out-of-phase ν_{2-} bending peak decreases in intensity and becomes almost unrecognizable in the 37.7- and 39.1-GPa spectra. As mentioned above, the dipole-dipole interaction is enhanced with pressure. This enhancement of the dipole-dipole interaction is considered here to be the cause of the bending mode splitting. The degeneration of the out-of-phase ν_{2-} bending vibration in ice VII begins at pressures above 30 GPa, and therefore is essentially related to the low-temperature ice-VII to ice-VIII transition below 100 K. For ice VII, the degeneration of the out-of-phase ν_{2-} bending vibration can be understood as a result of the dynamic rotation of molecules due to dipole-dipole interaction. The rotational tunneling that leads to the low-temperature ice-VII to ice-VIII transition at 30 GPa below 100 K is hence coupled with the out-of-phase ν_{2-} bending vibrational state. Theoretical studies have confirmed that defect motions in ice are coupled with vibrational states.[38,39]

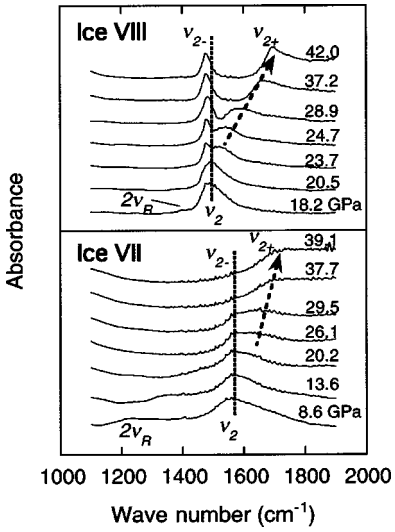

FIG. 6. Bending mode splitting for ice VIII at 20 K (top panel) and ice VII at 298 K (lower panel). For ice VIII, the absorption peak of the ν_2 bending mode, which is located at about 1500 cm^{-1} in the spectra below 21 GPa, splits into two peaks, assigned as the out-of-phase ν_{2-} and in-phase ν_{2+} bending vibrations, respectively, in the spectra above 23 GPa. For ice VII, the ν_2 bending mode splitting is clearly observed at pressures above 26 GPa. In the spectra above 23 GPa, the absorption peak of the in-phase ν_{2+} bending vibration overlaps with that of the $2\nu_R$ overtone. Dotted lines and dashed arrows are guides only.

In ice VII, oxygen atoms are arranged in a bcc structure but molecules are orientationally disordered. The present IR study of low-temperature ice VII and its metastability helps us to understand the nature of orientational disordering in ice VII. Orientational disordering in ice VII can be understood as thermally activated rotational disordering at pressures below 30 GPa and as rotational tunneling coupled with the bending vibrational states at pressures above 30 GPa. The degeneration of the out-of-phase ν_{2-} bending vibration is inferred to be caused by rotational tunneling. It is very interesting that in ice VIII with a displacement between two Ic networks the dipole-dipole interaction between the two Ic networks is buffered, and orientation and multisite disordering completely disappears.

ACKNOWLEDGMENTS

We thank Y. Matsushita, A. Nakayama, and E. Katoh for their assistance. This work was conducted under the Core Research for Evolutional Science and Technology (CREST) project supported by the Japan Science and Technology Corporation (JST).

[1] O. Mishima, L. D. Calvert, and E. Whalley, Nature (London) **310**, 393 (1984).
[2] R. J. Hemley, L. C. Chen, and H. K. Mao, Nature (London) **338**, 638 (1989).
[3] W. B. Holzapfel, J. Chem. Phys. **56**, 712 (1971); K. Schweizer and F. H. Stillinger, *ibid.* **80**, 1230 (1984); P. G. Johannsen, J. Phys.: Condens. Matter **10**, 2241 (1998); M. Benoit, D. Marx, and M. Parrinello, Nature (London) **392**, 258 (1998); M. Benoit, A. H. Romero, and D. Marx, Phys. Rev. Lett. **89**, 145501 (2002).
[4] Ph. Pruzan, J. Mol. Struct. **322**, 279 (1994).
[5] K. Aoki, H. Yamawaki, M. Sakashita, and H. Fujihisa, Phys. Rev. B **54**, 15 673 (1996); A. F. Goncharov, V. V. Struzhkin, M. S. Somayazulu, R. J. Hemley, and H. K. Mao, Science **273**, 218 (1996); A. F. Goncharov, V. V. Struzhkin, H. K. Mao, and R. J. Hemley, Phys. Rev. Lett. **83**, 1998 (1999).
[6] K. Aoki, H. Yamawaki, H. Fujihisa, and M. Sakashita, Science **268**, 1322 (1995).
[7] V. V. Struzhkin, A. F. Goncharov, R. J. Hemley, and H. K. Mao, Phys. Rev. Lett. **78**, 4446 (1997).
[8] M. Song, H. Yamawaki, H. Fujihisa, M. Sakashita, and K. Aoki, Phys. Rev. B **60**, 12 644 (1999).
[9] W. F. Kuhs, J. L. Finney, C. Vettier, and D. V. Bliss, J. Chem. Phys. **81**, 3612 (1984).
[10] E. Katoh, H. Yamawaki, H. Fujihisa, M. Sakashita, and K. Aoki, Science **295**, 1264 (2002).
[11] R. J. Nelmes, J. S. Loveday, R. M. Wilson, J. M. Besson, Ph. Pruzan, S. Klotz, G. Hamel, and S. Hull, Phys. Rev. Lett. **71**, 1192 (1993).
[12] R. J. Nelmes, J. S. Loveday, W. G. Marshall, G. Hamel, J. M. Besson, and S. Klotz, Phys. Rev. Lett. **81**, 2719 (1998).
[13] Ph. Pruzan, J. C. Chervin, and B. Canny, J. Chem. Phys. **99**, 9842 (1993); Ph. Pruzan, E. Wolanin, M. Gauthier, J. C. Chervin, B. Canny, D. Hausermann, and M. Hanfland, J. Phys. Chem. B **101**, 6230 (1997).
[14] R. J. Hemley, A. P. Jephcoat, H. K. Mao, C. S. Zha, L. W. Finger, and D. E. Cox, Nature (London) **330**, 737 (1987); J. Hama and K. Suito, Phys. Lett. A **187**, 346 (1994); E. Wolanin, Ph. Pruzan, J. C. Chervin, B. Canny, M. Gauthier, D. Hausermann, and M. Hanfland, Phys. Rev. B **56**, 5781 (1997).
[15] P. Loubeyre, R. LeToullec, E. Wolanin, M. Hanfland, and D. Hausermann, Nature (London) **397**, 503 (1999).
[16] J. S. Tse, D. D. Klug, C. A. Tulk, I. Swainson, E. C. Svensson, C.-K. Loong, V. Shpakov, V. R. Belosludov, R. V. Belosludov, and Y. Kawazoe, Nature (London) **400**, 647 (1999).
[17] J. L. Finney, C. Lobban, S. Klotz, and J. M. Besson, in *Collected Abstracts of the XVII Congress and General Assembly*, edited by J. F. Griffin (IUCr, Seattle, 1996), C-534.
[18] J. L. Finney, C. Lobban, S. Klotz, J. M. Besson, and G. Hamel, in *ISIS 96-Rutherford Appleton Laboratory Report*, edited by A. D. Taylor (Chilton, England, 1996), Vol. A17, RAL-96-050.
[19] S. Klotz, J. M. Besson, G. Hamel, R. J. Nelmes, J. S. Loveday, and W. G. Marshall, Nature (London) **398**, 681 (1999).
[20] S. Klotz *et al.*, Z. Kristallogr. **218**, 117 (2003).
[21] Ice VII-like phases can be produced by compressing ices II, V, VI, IX, XII, and HDA at low temperatures. According to neutron-diffraction measurements, the VII-like phase obtained from ice VI is identical to ice VII, but those obtained from other ice phases contain some non-VII features (see Refs. 17–20). These VII-like phases are indistinguishable by Raman-scattering and present IR measurements (see Ref. 2). Here we generally denote them as low-temperature ice VII and neglect the non-VII features in those VII-like phases produced by ices II, V, IX, XII, and HDA.
[22] J. S. Tse and M. L. Klein, Phys. Rev. Lett. **58**, 1672 (1987).
[23] H. K. Mao, J. Xu, and P. M. Bell, J. Geophys. Res., [Solid Earth] **91**, 4673 (1986).
[24] J. E. Bertie and E. Whalley, J. Chem. Phys. **40**, 1037 (1964).
[25] J. E. Bertie and E. Whalley, J. Chem. Phys. **40**, 1046 (1964).
[26] H. Engelhardt and E. Whalley, J. Chem. Phys. **71**, 4050 (1979).
[27] W. B. Holzapfel, B. Seiler, and M. Nicol, J. Geophys. Res. **89**, B706 (1984).
[28] M. Song, H. Yamawaki, H. Fujihisa, M. Sakashita, and K. Aoki, Phys. Rev. B **68**, 014106 (2003).
[29] At pressures below 23 GPa, the ν_2 bending modes of ices VII and VIII are located approximately at 1570 and 1500 cm^{-1}, respectively. At pressures above 23 GPa, a splitting of the ν_2 bending mode was observed (see details in Sec. IV and Fig. 6), and the bending frequency-pressure curves at 1570 and 1480 cm^{-1} are assigned as those of the out-of-phase vibration of the ν_2 bending mode of ices VII and VIII, respectively.
[30] B. Kamb, Acta Crystallogr. **17**, 1437 (1964).
[31] E. Whalley, *The Hydrogen Bond*, edited by P. Schuster, G. Zundel, and C. Sandorfy (North-Holland, Amsterdam, 1976), p. 1425.
[32] M. G. Sceats and S. A. Rice, in *Water, A Comprehensive Treatise*, edited by F. Franks (Plenum, New York, 1982), Vol. 7, p. 83.
[33] S. Kawada, J. Phys. Soc. Jpn. **44**, 1881 (1978).
[34] O. Haida, T. Matsuo, S. Hiroshi, and S. Seiki, J. Chem. Thermodyn. **6**, 815 (1974).
[35] W. B. Holzapfel, Physica B **265**, 113 (1999).
[36] The hydrogen-bonded O-O distance was calculated by the formulas in the Appendix of Ref. 4. Here we assume that the O-O distance in low-temperature ice VII is the same as that in ice VII.
[37] F. F. Muguet, J. Mol. Struct.: THEOCHEM **368**, 173 (1996).
[38] N. Bjerrum, Science **115**, 385 (1952).
[39] R. Podeszwa and V. Bush, Phys. Rev. Lett. **83**, 4570 (1999).